EUROPEAN ORGANISATION FOR PARTICLE PHYSICS

CERN-PPE/94-48
22 March 1994

Search for the Minimal Standard Model Higgs Boson

The OPAL Collaboration

Abstract

A search for the Minimal Standard Model Higgs boson (H^0) has been performed with data from e^+e^- collisions collected by the OPAL detector at LEP. The search was made for events of the types $e^+e^- \to (e^+e^-,\ \mu^+\mu^-$ or $\nu\bar{\nu})H^0$, $H^0 \to q\bar{q}$ and was based on approximately 78 pb^{-1} of data taken at center-of-mass energies between 88 and 95 GeV in the years 1990–1993. The present study, combined with previous OPAL publications, excludes the existence of a Minimal Standard Model Higgs boson with mass below 56.9 GeV at the 95% confidence level.

(Submitted to Physics Letters B)

The OPAL Collaboration

R. Akers[16], G. Alexander[23], J. Allison[16], K.J. Anderson[9], S. Arcelli[2], S. Asai[24], A. Astbury[28], D. Axen[29], G. Azuelos[18,a], A.H. Ball[17], R.J. Barlow[16], S. Barnett[16], R. Bartoldus[3], J.R. Batley[5], G. Beaudoin[18], A. Beck[23], G.A. Beck[13], J. Becker[10], C. Beeston[16], T. Behnke[27], K.W. Bell[20], G. Bella[23], P. Bentkowski[18], P. Berlich[10], S. Bethke[32], O. Biebel[3], I.J. Bloodworth[1], P. Bock[11], B. Boden[3], H.M. Bosch[11], M. Boutemeur[18], P. Bright-Thomas[25], R.M. Brown[20], A. Buijs[8], H.J. Burckhart[8], C. Burgard[27], P. Capiluppi[2], R.K. Carnegie[6], A.A. Carter[13], J.R. Carter[5], C.Y. Chang[17], C. Charlesworth[6], D.G. Charlton[8], S.L. Chu[4], P.E.L. Clarke[15], J.C. Clayton[1], I. Cohen[23], J.E. Conboy[15], M. Cooper[22], M. Coupland[14], M. Cuffiani[2], S. Dado[22], C. Dallapiccola[17], G.M. Dallavalle[2], C. Darling[31], S. De Jong[13], L.A. del Pozo[5], H. Deng[17], M. Dittmar[4], M.S. Dixit[7], E. do Couto e Silva[12], J.E. Duboscq[8], E. Duchovni[26], G. Duckeck[8], I.P. Duerdoth[16], D.J.P. Dumas[6], P.A. Elcombe[5], P.G. Estabrooks[6], E. Etzion[23], H.G. Evans[9], F. Fabbri[2], B. Fabbro[21], M. Fierro[2], M. Fincke-Keeler[28], H.M. Fischer[3], R. Folman[26], D.G. Fong[17], M. Foucher[17], H. Fukui[24], A. Fürtjes[8], A. Gaidot[21], J.W. Gary[4], J. Gascon[18], N.I. Geddes[20], C. Geich-Gimbel[3], S.W. Gensler[9], F.X. Gentit[21], T. Geralis[20], G. Giacomelli[2], P. Giacomelli[4], R. Giacomelli[2], V. Gibson[5], W.R. Gibson[13], J.D. Gillies[20], J. Goldberg[22], D.M. Gingrich[30,a], M.J. Goodrick[5], W. Gorn[4], C. Grandi[2], F.C. Grant[5], J. Hagemann[27], G.G. Hanson[12], M. Hansroul[8], C.K. Hargrove[7], P.F. Harrison[13], J. Hart[8], P.A. Hart[9], P.M. Hattersley[1], M. Hauschild[8], C.M. Hawkes[8], E. Heflin[4], R.J. Hemingway[6], G. Herten[10], R.D. Heuer[8], J.C. Hill[5], S.J. Hillier[8], T. Hilse[10], D.A. Hinshaw[18], P.R. Hobson[25], D. Hochman[26], R.J. Homer[1], A.K. Honma[28,a], R.E. Hughes-Jones[16], R. Humbert[10], P. Igo-Kemenes[11], H. Ihssen[11], D.C. Imrie[25], A. Jawahery[17], P.W. Jeffreys[20], H. Jeremie[18], M. Jimack[1], M. Jones[6], R.W.L. Jones[8], P. Jovanovic[1], C. Jui[4], D. Karlen[6], K. Kawagoe[24], T. Kawamoto[24], R.K. Keeler[28], R.G. Kellogg[17], B.W. Kennedy[15], J. King[13], S. Kluth[5], T. Kobayashi[24], M. Kobel[10], D.S. Koetke[8], T.P. Kokott[3], S. Komamiya[24], R. Kowalewski[8], R. Howard[29], J. von Krogh[11], J. Kroll[9], P. Kyberd[13], G.D. Lafferty[16], H. Lafoux[8], R. Lahmann[17], J. Lauber[8], J.G. Layter[4], P. Leblanc[18], P. Le Du[21], A.M. Lee[31], E. Lefebvre[18], M.H. Lehto[15], D. Lellouch[26], C. Leroy[18], J. Letts[4], L. Levinson[26], Z. Li[12], S.L. Lloyd[13], F.K. Loebinger[16], G.D. Long[17], B. Lorazo[18], M.J. Losty[7], X.C. Lou[8], J. Ludwig[10], A. Luig[10], M. Mannelli[8], S. Marcellini[2], C. Markus[3], A.J. Martin[13], J.P. Martin[18], T. Mashimo[24], P. Mättig[3], U. Maur[3], J. McKenna[29], T.J. McMahon[1], J.R. McNutt[25], F. Meijers[8], F.S. Merritt[9], H. Mes[7], A. Michelini[8], R.P. Middleton[20], G. Mikenberg[26], J. Mildenberger[6], D.J. Miller[15], R. Mir[12], W. Mohr[10], C. Moisan[18], A. Montanari[2], T. Mori[24], M. Morii[24], U. Müller[3], B. Nellen[3], H.H. Nguyen[9], S.W. O'Neale[1], F.G. Oakham[7], F. Odorici[2], H.O. Ogren[12], C.J. Oram[28,a], M.J. Oreglia[9], S. Orito[24], J.P. Pansart[21], P. Paschievici[26], G.N. Patrick[20], M.J. Pearce[1], P. Pfister[10], J.E. Pilcher[9], J. Pinfold[30], D. Pitman[28], D.E. Plane[8], P. Poffenberger[28], B. Poli[2], T.W. Pritchard[13], H. Przysiezniak[18], G. Quast[27], M.W. Redmond[8], D.L. Rees[8], G.E. Richards[16], M. Rison[5], S.A. Robins[13], D. Robinson[5], A. Rollnik[3], J.M. Roney[28], E. Ros[8], S. Rossberg[10], A.M. Rossi[2], M. Rosvick[28], P. Routenburg[30], K. Runge[10], O. Runolfsson[8], D.R. Rust[12], M. Sasaki[24], C. Sbarra[2], A.D. Schaile[26], O. Schaile[10], F. Scharf[3], P. Scharff-Hansen[8], P. Schenk[4], B. Schmitt[3], H. von der Schmitt[11], M. Schröder[12], H.C. Schultz-Coulon[10], P. Schütz[3], M. Schulz[8], C. Schwick[27], J. Schwiening[3], W.G. Scott[20],

M. Settles[12], T.G. Shears[5], B.C. Shen[4], C.H. Shepherd-Themistocleous[7], P. Sherwood[15], G.P. Siroli[2], A. Skillman[16], A. Skuja[17], A.M. Smith[8], T.J. Smith[28], G.A. Snow[17], R. Sobie[28], R.W. Springer[17], M. Sproston[20], A. Stahl[3], C. Stegmann[10], K. Stephens[16], J. Steuerer[28], R. Ströhmer[11], D. Strom[19], H. Takeda[24], S. Tarem[8], M. Tecchio[9], P. Teixeira-Dias[11], N. Tesch[3], M.A. Thomson[15], E. Torrente-Lujan[22], S. Towers[6], N.J. Tresilian[16], T. Tsukamoto[24], M.F. Turner[8], D. Van den plas[18], R. Van Kooten[12], G.J. VanDalen[4], G. Vasseur[21], M. Vincter[28], A. Wagner[27], D.L. Wagner[9], C. Wahl[10], C.P. Ward[5], D.R. Ward[5], J.J. Ward[15], P.M. Watkins[1], A.T. Watson[1], N.K. Watson[7], P. Weber[6], P.S. Wells[8], N. Wermes[3], B. Wilkens[10], G.W. Wilson[4], J.A. Wilson[1], V-H. Winterer[10], T. Wlodek[26], G. Wolf[26], S. Wotton[11], T.R. Wyatt[16], R. Yaari[26], A. Yeaman[13], G. Yekutieli[26], M. Yurko[18], W. Zeuner[8], G.T. Zorn[17].

[1]School of Physics and Space Research, University of Birmingham, Birmingham B15 2TT, UK
[2]Dipartimento di Fisica dell' Università di Bologna and INFN, I-40126 Bologna, Italy
[3]Physikalisches Institut, Universität Bonn, D-53115 Bonn, Germany
[4]Department of Physics, University of California, Riverside CA 92521, USA
[5]Cavendish Laboratory, Cambridge CB3 0HE, UK
[6]Carleton University, Department of Physics, Colonel By Drive, Ottawa, Ontario K1S 5B6, Canada
[7]Centre for Research in Particle Physics, Carleton University, Ottawa, Ontario K1S 5B6, Canada
[8]CERN, European Organisation for Particle Physics, CH-1211 Geneva 23, Switzerland
[9]Enrico Fermi Institute and Department of Physics, University of Chicago, Chicago IL 60637, USA
[10]Fakultät für Physik, Albert Ludwigs Universität, D-79104 Freiburg, Germany
[11]Physikalisches Institut, Universität Heidelberg, D-69120 Heidelberg, Germany
[12]Indiana University, Department of Physics, Swain Hall West 117, Bloomington IN 47405, USA
[13]Queen Mary and Westfield College, University of London, London E1 4NS, UK
[14]Birkbeck College, London WC1E 7HV, UK
[15]University College London, London WC1E 6BT, UK
[16]Department of Physics, Schuster Laboratory, The University, Manchester M13 9PL, UK
[17]Department of Physics, University of Maryland, College Park, MD 20742, USA
[18]Laboratoire de Physique Nucléaire, Université de Montréal, Montréal, Quebec H3C 3J7, Canada
[19]University of Oregon, Department of Physics, Eugene OR 97403, USA
[20]Rutherford Appleton Laboratory, Chilton, Didcot, Oxfordshire OX11 0QX, UK
[21]DAPNIA/SPP, Saclay, F-91191 Gif-sur-Yvette, France
[22]Department of Physics, Technion-Israel Institute of Technology, Haifa 32000, Israel
[23]Department of Physics and Astronomy, Tel Aviv University, Tel Aviv 69978, Israel
[24]International Centre for Elementary Particle Physics and Department of Physics, University of Tokyo, Tokyo 113, and Kobe University, Kobe 657, Japan
[25]Brunel University, Uxbridge, Middlesex UB8 3PH, UK
[26]Particle Physics Department, Weizmann Institute of Science, Rehovot 76100, Israel

[27]Universität Hamburg/DESY, II Institut für Experimental Physik, Notkestrasse 85, D-22607 Hamburg, Germany
[28]University of Victoria, Department of Physics, P O Box 3055, Victoria BC V8W 3P6, Canada
[29]University of British Columbia, Department of Physics, Vancouver BC V6T 1Z1, Canada
[30]University of Alberta, Department of Physics, Edmonton AB T6G 2J1, Canada
[31]Duke University, Dept of Physics, Durham, NC 27708-0305, USA
[32]Universität Aachen, III Physikalisches Institut, Sommerfeldstrasse 26-28, D-52056 Aachen, Germany

[a]Also at TRIUMF, Vancouver, Canada V6T 2A3

1 Introduction

Local gauge invariant theories of the electroweak interaction introduce spontaneous symmetry breaking [1] in order to allow the gauge bosons to acquire mass while keeping the theory renormalizable. This procedure predicts the existence of one or more scalar particles - the Higgs bosons [2]. These Higgs particles have not yet been observed.

The simplest such model, the Minimal Standard Model, has one doublet of complex Higgs fields. It predicts the existence of a single scalar Higgs boson (H^0) with an unspecified mass but well defined couplings. Consequently, the cross section for the production of an H^0 at LEP (through the Bjorken process $e^+e^- \to Z^0 \to Z^* H^0$ [3]) and the H^0 decay modes are precisely predicted as a function of the Higgs boson mass.

The results of earlier searches for a Higgs boson have been published by OPAL [4, 5] and by the other LEP experiments [6]. The present paper makes use of a data sample of about 1.9 million reconstructed hadronic Z^0 events, which were collected by the OPAL experiment between 1990 and 1993. The analysis is performed for the "neutrino channel" ($Z^* \to \nu\bar{\nu}$ and $H^0 \to q\bar{q}$) and the "charged lepton channel" ($Z^* \to e^+e^-$ or $\mu^+\mu^-$ and $H^0 \to q\bar{q}$). Other channels previously exploited, namely, $Z^* \to \tau^+\tau^-$ and $H^0 \to q\bar{q}$, $Z^* \to q\bar{q}$ and $H^0 \to \tau^+\tau^-$ and $Z^* \to \nu\bar{\nu}$ and $H^0 \to \tau^+\tau^-$ have been discarded because, for heavy (≈ 60 GeV) Higgs bosons, the number of signal and background events is expected to be comparable.

Previously published search strategies adopted by OPAL [4, 5], were optimized for H^0 with mass up to about 40 GeV. In order to extend the search sensitivity to higher mass, the analysis has been reoptimized to exploit detector improvements, improved event reconstruction and better understanding of the detector response, while the rejection of background events has been increased.

2 The OPAL Detector

The OPAL detector, which is described in detail in [7], is a solenoidal detector with a pressurized central tracking system operating in a 0.435 T magnetic field. The lead-glass electromagnetic calorimeter together with presamplers and time-of-flight scintillators are located outside the magnet coil and pressure vessel. The magnet return yoke is instrumented for hadron calorimetry and is surrounded by external muon chambers. Forward calorimeters close to the beam axis measure luminosity and complete the acceptance. The detector features of relevance to this analysis are described briefly below.

A right-handed coordinate system is adopted, where the x axis points to the center of the LEP ring, and positive z is along the electron beam direction. The angles θ and ϕ are the polar and azimuthal angles, respectively.

The central tracking system consists of a silicon micro-vertex detector, a vertex drift cham-

ber, a jet chamber and a system of chambers which measure the z coordinate.

In the range $|\cos\theta| < 0.73$, 159 points are measured in the jet chamber along each track and at least 20 points on a track are obtained over 96% of the full solid angle. The momentum in the r-ϕ plane, p_t, is measured with a resolution of $(\sigma(p_t)/p_t)^2 = 0.02^2 + (0.0015 \cdot p_t)^2$, ($p_t$ in GeV) for $|\cos\theta| < 0.73$. The jet chamber also provides measurements of the ionization, $\mathrm{d}E/\mathrm{d}x$, of charged tracks. The average resolution is 3.5% for 159 samples [8].

Electron and photon energies are measured by the barrel and endcap lead-glass electromagnetic calorimeters. These detectors cover the full azimuth in the polar angle range of $|\cos\theta| < 0.84$ for the barrel and $0.81 < |\cos\theta| < 0.984$ for the endcaps. The forward detectors on both sides of the interaction point cover the polar angle region between 34 and 120 mrad. When high energy electrons or photons are incident on the gap of 0.8% in solid angle between the endcap lead-glass and the forward detector, some fraction of the shower is usually detected at the edge of one of these calorimeters. Thus, photons and electrons are detected with an acceptance of almost 4π. The barrel lead-glass blocks have a pointing geometry. To achieve good hermeticity, the small 1 mm gaps between the lead-glass blocks do not point exactly to the interaction point. The intrinsic energy resolution of the calorimeter is $5\text{–}6\%/\sqrt{E}$ which is degraded by about a factor of two by the material of the magnet coil and the pressure vessel in front of the calorimeter. The effect of material is more significant in the region near the overlap of the barrel and the endcap calorimeters ($0.72 < |\cos\theta| < 0.84$). The angular resolution of electromagnetic clusters is approximately 4 mrad both in θ and ϕ for energies above 10 GeV.

The hadron calorimeter is made up of three sections: the barrel, the endcap and the pole tip, which together cover the region $|\cos\theta| < 0.99$. The magnet return yoke is instrumented with limited streamer tubes in the barrel and endcap sections, and with thin, high gain chambers in the pole tips. There are nine layers of chambers in the barrel, eight in the endcap, and ten in the pole tips. These are read out with narrow strips, and by pads which are grouped together to form towers. The strips are used for tracking, and for muon identification. The towers are used for energy measurement, for which the resolution is $\sigma/E = 120\%/\sqrt{E}$.

There are at least seven, and in most regions eight, absorption lengths of material between the interaction point and the muon detectors. Muons with momenta above 3 GeV usually penetrate to the muon chambers. The muon barrel detector covers the region $|\cos\theta| < 0.7$. It is composed of four layers of planar drift chambers, with cylindrical geometry. These give a position accuracy of 1.5 mm in r–ϕ and 2 mm in z. The muon endcap detector covers the polar angle range $0.67 < |\cos\theta| < 0.98$. It is composed of two planes of limited streamer tube arrays at each end of the detector, yielding resolutions of 1–3 mm on the x and y coordinates. The z coordinate is known from the surveyed positions of the chambers. The two muon detector subsystems cover 93% of the full solid angle.

3 Data Sample and Simulation

About 1.9 million hadronic Z^0 decay events, corresponding to an integrated luminosity of 78 pb^{-1}, were collected by the OPAL experiment in the period 1990–1993. To ensure the reliability of the event reconstruction, data were used only if all major components of the detector were fully operational. The tracks used in the analysis were required to originate at the interaction point, to have a minimum number of hits in the jet chamber, and to have a transverse momentum greater than 0.1 GeV. Energy clusters in the electromagnetic and hadron calorimeters were required to exceed minimum energy thresholds. The precise requirements on tracks and clusters are given in [5]. Spurious tracks with high momentum distort a number of variables, such as event acolinearity and acoplanarity, which were used in the analysis. To avoid such effects, events containing one or more tracks with momentum greater than 25 GeV, but which had a poor track fit, and events containing tracks with momentum greater than the beam momentum have been excluded from the analysis. This rejected 0.4% of the data.

An algorithm has been developed to calculate masses, energies and momenta, for any desired set of tracks and calorimeter clusters using information from all detector components, and which eliminates double counting the effects of tracks and clusters [5]. This algorithm, termed the GCE algorithm, was used to calculate variables required for the analysis described in the sections below. In particular it was used to calculate the observed mass of events, with a resolution $(\sigma_m/m) \approx 12\%$, and with a mass shift given by $m_{obs} = 0.87 \times m_{true}$.

Monte Carlo events for the main background process, $e^+e^- \rightarrow$ hadrons were generated using the JETSET [9] and HERWIG [10] programs and the detector response was simulated using the GOPAL program [11]. The generators were tuned to reproduce global event-shape variables measured with OPAL data [12]. Simulated signal events were produced by the generator described in [13], with some modifications to improve the efficiency of the calculation [14], and processed in the same manner as the data.

4 Search for $Z^0 \rightarrow \nu\bar{\nu}$ H^0, with $H^0 \rightarrow q\bar{q}$

The neutrino channel accounts for approximately 70% of the search sensitivity.

Unlike the case of the search for a lower mass H^0, missing energy becomes an unreliable indicator of the presence of a high mass H^0 because of the non-zero width of the missing energy distribution for hadronic Z^0 decays. The experimental signature of events containing Higgs bosons used in this analysis is a pair of jets which are not back-to-back.

To identify events with this topology, the analyzed events were split into two hemispheres using the plane orthogonal to the thrust axis. The momentum vector of each hemisphere was calculated and the acolinearity angle (θ_{acol}, the complement of the 3-dimensional angle between the two momentum vectors) and the acoplanarity angle (θ_{acop}, the complement of the angle between the projections of the two momentum vectors onto the plane perpendicular to

the beam direction) were computed. Momentum conservation in hadronic Z^0 decays keeps the observed hemisphere momentum vectors back-to-back: an event displaying a significant deviation from a back-to-back topology is either the result of energy loss down the beam-pipe or the presence of high energy neutrinos from heavy quark decays, or possibly due to the process $Z^* \rightarrow H^0 \nu\bar{\nu}$.

4.1 Selection Procedure

An initial selection of events having $\cos\theta_{acol} < 0.98$ was made in order to decrease the number of events to be analyzed.

The high track and cluster multiplicities of a heavy Higgs boson decay allow rejection of virtually all leptonic Z^0 decays, including most $\tau^+\tau^-$ events with a converting photon. The following requirements were made:

- Each event was required to contain at least seven charged tracks.
- Each event was required to contain at least seven clusters in the electromagnetic calorimeter.
- The thrust for events containing fewer than nine charged tracks was required to be less than 0.95.

The identification of signal events is based on their large acolinearity and acoplanarity angles. To ensure good energy containment, which is crucial for a reliable measurement of these angles, events with a large energy flow near the beam pipe were eliminated by the following cuts.

- The energy deposited in the forward calorimeters was required to be less than 2 GeV.
- The missing momentum direction was limited to the range $|\cos\theta_{p_{miss}}| < 0.94$, where $\theta_{p_{miss}}$ is the polar angle of the missing momentum vector.
- The forward energy flow, defined as $(E_F^2 + E_B^2)/E_{tot}^2$, was required to be less than 10. E_{tot} is the total energy of the event, E_F and E_B are the total weighted energies observed in the forward and backward cones defined by $|\cos\theta| > 0.8$. The energies of charged tracks and electromagnetic clusters with polar angle θ are weighted by $\sin^{-2}\theta$, which gives more importance to energy of tracks and clusters near the beam-pipe.
- The z-component of the total event momentum was required to be less than 20 GeV.

Background from two-photon interactions was reduced by:

- The invariant mass of the event was required to be greater than 25 GeV for events having a total transverse momentum, relative to the beam axis, less than 10 GeV.

The measurement of the acolinearity and acoplanarity angles is more accurate for two-jet events than for spherical events. To ensure accurate evaluation of these angles, spherical events were rejected by:

- The event thrust was required to be greater than 0.70.

Hadronic Z^0 decays with little missing energy had already been removed by the initial acolinearity selection, and the remaining events at this point were well-contained multi-jet events (having three or more jets). The missing momentum vector in jets with underestimated energy (due to the presence of energetic neutrinos coming from heavy flavor decays, or a poorly measured energetic neutral hadron) points along the direction of the jet, in contrast to H^0 events where the missing momentum vector points along the Z^* flight direction. Hadronic Z^0 decays with the energy of one jet underestimated were removed by requiring the missing-momentum vector to be isolated:

- The sum of the charged track energy and the cluster energy in the electromagnetic and hadron calorimeters was required to be less than 2.0 GeV in a cone of half-angle 45° around the missing-momentum vector.

The remaining background was from almost back-to-back Z^0 multi-jet events with energy in more than one jet underestimated. These events were removed by the stringent acolinearity and acoplanarity requirements given below. The widths of the distributions of these variables depended both on the location of the tracks and clusters in the detector, and on the shape of the event, and thus on the selection requirements.

The GCE algorithm was used to calculate the mass and thrust for each hemisphere using tracks and clusters of that hemisphere. Higgs events, which generally contain one jet per hemisphere, are characterised by a relatively low reconstructed hemisphere mass, and high hemisphere thrust. Multi-jet events have at least one hemisphere with more than one jet. These hemispheres are characterized by relatively high reconstructed mass, and low hemisphere thrust.

The average of the two hemisphere masses, m_{hemi}^{avg}, is used together with the lower of the two thrust values calculated for each hemisphere separately, T_{hemi}^{min}, to separate events into three classes. The first has a clear two-jet topology (class A) and contains 75% of the signal for a H^0 of mass 60 GeV. It is defined by:

- Class A is the region m_{hemi}^{avg}<11 GeV and T_{hemi}^{min}>0.85.

In this class a small deviation from a back-to-back topology is enough to tag an event as a Higgs boson candidate. The second class (class B) contains events with an ambiguous jet topology and is defined by:

- Class B is the region m_{hemi}^{avg}<20 GeV and T_{hemi}^{min}>0.70 (excluding class A).

In this class, which contains 24% of the signal, a larger deviation from a back-to-back topology is required. Events in neither of the above classes (about 1% of the signal) have a clear multi-jet topology which prevents a reliable separation of signal from background, and are not accepted.

In general, the acolinearity and acoplanarity angles are better measured when both hemisphere momentum vectors are in the barrel region ($135° > \theta > 45°$). The superior resolution in the barrel allows looser cuts on the signal in this region compared to the cuts required for the endcap region. The numerical values of the acolinearity and acoplanarity cuts applied in the two regions are given in table 1 below.

Classes A and B as defined above are outlined in figure 8, which shows the m_{hemi}^{avg} versus T_{hemi}^{min} distribution of a 60 GeV Higgs boson signal, together with the same distribution for data events. The initial acolinearity cut removed most of the Z^0 hadronic decay events that would otherwise fall into class A. In figure 8, $\cos\theta_{acol}$ is plotted against $\cos\theta_{acop}$ for all events belonging to each class, together with simulated hadronic Z^0 decay events. H^0 events are characterized by much broader $\cos\theta_{acol}$ and $\cos\theta_{acop}$ distributions than the background and a sizeable fraction of the signal events is accepted by these cuts.

Table 2 gives the number of events for the data, simulated hadronic Z^0 decays and simulated H^0 events after the successive cuts of the neutrino channel analysis.

One event, with mass (after taking into account the systematic shift discussed in section 3) of 28.9 $\pm$3.5 GeV was selected by these cuts. Higgs bosons in this mass region have been already excluded in previous OPAL publications [4, 5]. As the mass of this event is far from the current mass limit, in terms of mass resolution, the effect of this candidate on the present lower mass bound is negligible.

4.2 Background and Systematic Error Estimation

The dominant background is from hadronic Z^0 decays, with final states containing either very energetic neutrinos, or very energetic, long-lived neutral hadrons mismeasured in the hadron calorimeter.

A large sample of inclusive hadronic Z^0 decays was generated consisting of approximately 1.4M JETSET events together with a sample of approximately 0.3M HERWIG events. In addition, a sample of events pre-selected at the generator level for the presence of a high energy neutral hadron or neutrino has been analysed. This sample corresponded to 33M Z^0 decays. Four simulated events survived the analysis cuts, of which one came from the inclusive sample,

and contained an energetic K_L. The expected background from this source is estimated to be 0.15 events. The number of simulated events passing the analysis cuts is small compared to the size of the simulated event sample, and unknown systematic effects in the simulations preclude evaluating a realistic error on the background estimate. Two photon events were not simulated, but are not expected to give rise to high mass hadronic systems.

The systematic uncertainties are summarized below:

- luminosity: 1.3%.
- signal selection efficiency: 1.8%.
- Higgs boson production cross-section: 1%.

Summed in quadrature, the overall uncertainty is 2.4%. Table 3 gives the efficiencies of the neutrino channel search for various Higgs boson masses. To avoid an overestimation of the numbers of expected events due to systematic effects, these numbers have been reduced by one standard deviation of the systematic error.

The present analysis excludes a Minimal Standard Model Higgs boson with mass up to 57.5 GeV at the 95% confidence level, using the neutrino channel alone.

5 Search for $Z^0 \rightarrow (e^+e^- \text{or } \mu^+\mu^-)H^0$, with $H^0 \rightarrow q\bar{q}$

The experimental signature for Minimal Standard Model Higgs boson events in the charged lepton channel is a pair of well isolated energetic charged leptons produced together with a high mass hadronic system. Only electron and muon pairs have been considered in this analysis. Four-fermion processes [15, 16] give rise to background in this channel.

5.1 Selection Procedure

An initial selection was made to reduce the number of events to be studied in the later stages of the analysis. The preselection requirements were as follows.

- The lepton tracks were required to have opposite charge.
- The lepton track momenta were required to be above 3.0 GeV.
- The opening angle between the lepton tracks was required to be greater than 30°.

The electron preselection requirements were as follows.

- Each electron track was required to be associated with a cluster in the electromagnetic calorimeter. The azimuthal angle of the track, at the entrance to the calorimeter, was required to be within 20 mrad of the cluster.
- The cluster energies were each required to be above 3.0 GeV.
- The sum of the two cluster energies was required to be greater than 20.0 GeV.

The muon preselection requirements were:

- Each muon track was required to be associated with a cluster in the electromagnetic calorimeter. The azimuthal angle of the track, at the entrance to the calorimeter, was required to be within 150 mrad of the cluster.
- At least one of the muon tracks was required to have more than four hits in the hadron calorimeter.
- Each track was required to have two or more hits in the last five layers of the hadron calorimeter, or two or more hits in the surrounding muon chambers.
- The scalar sum of the momenta of the two muon tracks was required to be greater than 20.0 GeV.

The events were then subject to the following cuts common to the electron and muon channel analyses.

- Each lepton track was required to have a momentum greater than 5.0 GeV.
- Each lepton track was required to have $\mid \cos\theta \mid \leq 0.92$.
- The event was required to have more than three tracks excluding those within 15° of the lepton tracks, and excluding the lepton tracks.
- The event was required to have more than five clusters in the electromagnetic calorimeter.
- The event was required to have less than 2.0 GeV deposited in the Forward Detectors.

The pair was identified as a $\mu^+\mu^-$ pair if:

- The scalar sum of the momenta of the two tracks was greater than 25.0 GeV.
- Each track was associated with a track segment in the hadron calorimeter seen in at least three out of the outer five strip layers.
- At least one of the tracks was associated with a track segment in the muon chambers seen in at least three of the four planes.

- The sum of the electromagnetic calorimeter energies associated with the tracks was less than 5 GeV.

The pair was identified as an e^+e^- pair if:

- Each of the two tracks had an associated electromagnetic calorimeter cluster with energy of at least 5 GeV, with 90% of this energy contained in less than 5 lead-glass blocks.
- Any hadron calorimeter cluster associated with the tracks had an energy less than 4 GeV.
- The sum of the energies of the two associated electromagnetic calorimeter clusters was at least 25 GeV.
- The $\mathrm{d}E/\mathrm{d}x$ of tracks with momentum less than 15 GeV and at least 40 $\mathrm{d}E/\mathrm{d}x$ hits, was required to be consistent with electrons, *i.e.* it was required to be greater than 9.17 keV/cm, which is two standard deviations below the mean $\mathrm{d}E/\mathrm{d}x$ for electrons.
- The E/p ratio of tracks satisfying $|\cos\theta| \leq 0.72$ or $|\cos\theta| \geq 0.84$ was required to exceed 0.7. The cut was not applied in the region $0.72 < |\cos\theta| < 0.84$ where the presence of extra material degrades the energy measurement.

Each of the two candidate charged lepton tracks was required to be isolated from other tracks and clusters in the event. The following two tests of the lepton track isolation were performed:

- The scalar momenta of charged tracks in a cone of half-angle 30° about each lepton track, excluding the lepton momenta, were summed. The ratio of this sum to the sum of the scalar momenta of tracks in the event, excluding the lepton momenta, was required to be less than 0.2. The test was repeated using clusters in the electromagnetic calorimeter instead of charged tracks.
- The previous isolation test was repeated using a cone of 45° about the higher momentum lepton track, and a cone of 15° about the lower momentum track.

The first test had a higher probability to select events for which the angle between the lepton pair and the Z^* flight direction, in the Z^* rest frame, was close to 90°, while the second test selected events where this angle was close to 0°. Events were kept for further analysis if they passed either isolation test. A final isolation requirement was made:

- The sum of the scalar momenta of tracks within 15° of the lepton tracks, but excluding the lepton tracks, was required to be less than 1 GeV.

If more than one lepton pair was found in an event, the pair with the smallest sum of charged track and electromagnetic cluster energies in 30° cones centered on the leptons (excluding the tracks and clusters associated with them) was chosen.

Figure 8 shows the lepton isolation quality in the data. Twenty-nine out of the 1970 events with two identified leptons survived the isolation cuts.

Four-fermion processes remained to be suppressed. In most four-fermion events, one fermion pair originates from the decay of the Z^0 and so has large mass, while the other pair originates from a virtual photon, and is characterized by a low mass. The momentum and opening angle cuts suppress events with low di-lepton mass and high hadronic mass. Figure 8 shows the mass of the lepton pair versus the hadronic mass after isolation cuts. Figure 8a shows the data while figure 8b shows the four-fermion events simulated with the generator FERMISV [17] for an integrated luminosity that corresponds to 100 times the integrated luminosity of the data sample. Detector simulation was not performed for these events. The distribution is seen to extend to high hadronic mass.

To reject four-fermion events, the following requirements were made:

- The invariant mass of the lepton pair was required to be greater than 15 GeV.
- The invariant mass of all tracks and clusters lying outside 15° cones about the lepton tracks was required to be greater than 25 GeV.

Tables 4 and 5 give the numbers of events for the data, for simulated hadronic Z^0 decays and for simulated H^0 events after the successive cuts of the electron and muon channel analyses.

One event is accepted by the charged lepton channel selection procedure. The event has two energetic isolated muons and a three-jet hadronic system. The muons are clearly identified by both the muon chambers and the hadronic calorimeter. They are well isolated, having no energy in a cone of 30° half-opening angle. The di-muon invariant mass is 16.6 ± 0.3 GeV and the mass of the hadronic system calculated from the recoil mass of the two muons is 61.2 ± 1.0 GeV. The mass of the hadronic system is measured to be 54 ± 7 GeV (after correction for the mass shift discussed in section 3).

There is some indication that the most energetic jet contains a heavy flavor hadron. It contains a significantly displaced secondary vertex (4.4 σ) with four charged tracks, one of which is a 1.5 GeV electron with associated hits in both silicon micro-vertex layers, and no accompanying positron candidate.

There is no clear indication of heavy flavor content in either of the other two jets. However, one of these jets has a low polar angle, and for this jet no reliable secondary vertex finding can be performed.

The event is shown in figure 8 and its properties are summarized in table 6.

5.2 Background and Systematic Error Estimation

The lepton identification procedure was applied to simulated Z^0 di-lepton events, and to di-lepton events in the data. The difference in the efficiencies of the procedure for these two event samples, which was found to be 7%, was used to correct the efficiency obtained for simulated Higgs boson events. The correction was calculated using mainly beam energy leptons, while the momentum dependence was studied using electrons and muons coming from tau decays. The correction factor determined in this manner is applicable to the efficiencies for Higgs boson events as the lepton pairs are isolated in all cases. The uncertainty in the correction was taken to be the systematic error on the lepton identification procedure. The contributions to the systematic errors are:

- Luminosity: 1.3%.
- Higgs boson production cross section: 1%.
- Final state radiation: 1%.
- Lepton identification: 0.8%.

which, added in quadrature, gives an overall uncertainty of 2.1%. Table 3 gives the efficiencies of the charged lepton channel search for various Higgs boson masses. To avoid an overestimation of the numbers of expected events due to systematic effects, these numbers have been reduced by one standard deviation of the systematic error.

The expected background in the charged lepton channel is from four-fermion events. For a hadronic mass greater than 25 GeV, 2.0 ± 0.7 events are expected. Only events with mass greater than 50 GeV would significantly affect the mass limit, and 0.5 ± 0.1 background events are expected in this region.

The present analysis excludes a Minimal Standard Model Higgs boson with mass up to 51.9 GeV, at the 95% confidence level, using the charged lepton channel alone.

6 Mass Limit

The efficiency for each decay channel and the number of expected events for several Higgs boson masses are shown in Table 3. The neutrino channel gives a 95% confidence level lower mass limit of 57.5 GeV, while the leptonic channel gives a lower mass limit of 51.9 GeV. The mass of the event which is observed in the leptonic channel is close to the combined limit. Due to a possible shift in recoil mass due to initial state radiation, a conservative approach was taken in combining the two channels. The limit was calculated in the presence of one candidate event, and no background events. This procedure resulted in a 95% C.L. lower mass limit for the Minimal Standard Model Higgs boson of 56.9 GeV. Figure 8 shows the number of expected events for the combined analysis, and in the two search channels separately.

7 Conclusion

A search has been made for the Minimal Standard Model Higgs boson with the OPAL detector at LEP using a data sample with an integrated luminosity of 78 pb^{-1}. The reactions used were $e^+e^- \to Z^*H^0$, $H^0 \to$hadrons and $Z^* \to (\nu\bar{\nu}$ or e^+e^- or $\mu^+\mu^-)$. The search has a high efficiency to detect the Higgs boson in the mass range 25 – 65 GeV. One event with mass 28.9±3.5 GeV passed the $Z^* \to \nu\bar{\nu}$ selection. One event with recoil mass 61.2±1.0 GeV passed the $Z^* \to \mu^+\mu^-$selection. The effect of the candidate with mass 28.9 GeV on the mass limit is negligible. The expected number of background events in the charged lepton channel for hadronic masses greater than 25 GeV is 2.0±0.7, of which 0.5±0.1 were expected to have a mass in excess of 50 GeV. The event observed in the charged lepton channel has a mass near the mass limit, and the conservative procedure of taking this event as a candidate event was followed. The new lower mass limit for the Minimum Standard Model Higgs boson was calculated to be 56.9 GeV at the 95% confidence level.

8 Acknowledgements

It is a pleasure to thank the SL Division for the efficient operation of the LEP accelerator, the precise information on the absolute energy, and their continuing close cooperation with our experimental group. In addition to the support staff at our own institutions we are pleased to acknowledge the
Department of Energy, USA,
National Science Foundation, USA,
Texas National Research Laboratory Commission, USA,
Science and Engineering Research Council, UK,
Natural Sciences and Engineering Research Council, Canada,
Fussefeld Foundation,
Israeli Ministry of Energy and Ministry of Science,
Minerva Gesellschaft,
Japanese Ministry of Education, Science and Culture (the Monbusho) and a grant under the Monbusho International Science Research Program,
German Israeli Bi-national Science Foundation (GIF),
Direction des Sciences de la Matière du Commissariat à l'Energie Atomique, France,
Bundesministerium für Forschung und Technologie, Germany,
National Research Council of Canada,
A.P. Sloan Foundation and Junta Nacional de Investigação Científica e Tecnológica, Portugal.

References

[1] S. L. Glashow, J. Iliopoulos and L. Maiani, Phys. Rev. **D2** (1970) 1285;
S. Weinberg, Phys. Rev. Lett. **19** (1967) 1264;
A. Salam, *Elementary Particle Theory*, ed. N. Svartholm (Almquist and Wiksells, Stockholm, 1968), 367.

[2] P. W. Higgs, Phys. Lett. **12** (1964) 132;
F. Englert and R. Brout, Phys. Rev. Lett. **13** (1964) 321;
G. S. Guralnik, C. R. Hagen, and T. W. B. Kibble, Phys. Rev. Lett. **13** (1964) 585.

[3] J. Bjorken, *Proceedings of the 1976 SLAC Summer Institute on Particle Physics*, SLAC-198 (1977) 1.

[4] OPAL Collab., M. Z. Akrawy *et al.*, Phys. Lett. **B236** (1990) 224;
OPAL Collab., M. Z. Akrawy *et al.*, Phys. Lett. **B251** (1990) 211;
OPAL Collab., M. Z. Akrawy *et al.*, Zeit. f. Phys. **C49** (1991) 1;
OPAL Collab., P. D. Acton *et al.*, Phys. Lett. **B268** (1991) 122.

[5] OPAL Collab., M. Z. Akrawy *et al.*, Phys. Lett. **B253** (1991) 511.

[6] ALEPH Collab., D. Buskulic *et al.*, Phys. Lett. **B313** (1993) 299;
DELPHI Collab., P. Abreu *et al.*, Nucl. Phys. **B373** (1992) 3;
L3 Collab., O. Adriani *et al.*, Phys. Lett. **B303** (1993) 391.

[7] OPAL Collaboration, K. Ahmet *et al.*, Nucl. Inst. Meth. **A305** (1991) 275.

[8] M. Hauschild *et al.*, Nucl. Instrum. Methods **A314** (1992) 74.

[9] JETSET, Version 7.3; T. Sjöstrand, Comp. Phys. Comm. **39** (1986) 347;
T. Sjöstrand and M. Bengtsson, Comp. Phys. Comm. **43** (1987) 367;
T. Sjöstrand, CERN-TH/6488/92.

[10] HERWIG, Version 5.5; G. Marchesini and B.R. Webber, Nucl. Phys. **B310** (1988) 461;
G. Marchesini *et al.*, Comp. Phys. Comm. **67** (1992) 465.

[11] J.Allison *et al.*, Nucl. Instrum. Methods **A317** (1992) 47.

[12] OPAL Collaboration, M.Z. Akrawy *et al.*, Z. Phys. **C47** (1990) 505;
OPAL Collaboration, P.D. Acton *et al.*, Z. Phys. **C58** (1993) 387.

[13] F.A. Berends and R. Kleiss, Nucl. Phys. **B260** (1985) 32.

[14] E. Gross, Ph.D. Thesis, Weizmann Institute, December 1990.

[15] F.A.Berends, P.H.Daverveldt and R.Kleiss, Nucl. Phys. **B253** (1985) 421.

[16] L3 Collaboration, A. Adam *et al.*, Phys. Lett. **B321** (1994) 283.

[17] J. Hilgart, R. Kleiss and F. Le Diberder, Comp. Phys. Comm. **75** (1993) 191.

Table 1: Class definitions and value of the cuts on the cosine of the acolinearity angle and the cosine of the acoplanarity angle, for the $\nu\bar{\nu}\mathrm{H}^0$ search.

Class	T_{hemi}^{min}	m_{hemi}^{avg}	region	$\cos\theta_{acol}$	$\cos\theta_{acop}$
A	0.85 - 1.00	0 - 11 GeV	barrel	< 0.95	< 0.98
			endcap	< 0.90	< 0.98
B	0.70 - 1.00	0 - 20 GeV			
(excluding class A)			barrel	< 0.85	< 0.95
			endcap	< 0.70	< 0.95

Table 2: Numbers of events after successive cuts in the neutrino channel, for the data, for simulated $\mathrm{Z}^0\to\mathrm{q\bar{q}}$ events and for a H^0 of mass 60 GeV. The numbers of simulated $\mathrm{Z}^0\to\mathrm{q\bar{q}}$ events have been scaled so that the real and simulated data sample sizes are the same. The numbers between parentheses give efficiencies.

Cuts	Data	$\mathrm{Z}^0\to\mathrm{q\bar{q}}$	$\nu\bar{\nu}\mathrm{H}^0$
Preselection	63776 (3.30%)	29830 (1.55%)	4.8 (83%)
Tau rejection	33909 (1.76%)	29163 (1.51%)	4.7 (82%)
Forward energy	17947 (0.93%)	17716 (0.92%)	4.1 (71%)
$\gamma\gamma$ rejection	17265 (0.89%)	17714 (0.91%)	4.1 (71%)
Thrust and Missing Momentum	1984 (0.10%)	2128 (0.11%)	2.6 (45%)
Acolinearity/acoplanarity	1 (0.00%)	1.4 (0.00%)	1.9 (33%)

Table 3: Efficiencies and expected number of events for the neutrino and charged lepton channels. The numbers of events have been reduced by the systematic error.

m_{H^0}(GeV)	$\epsilon^{\nu\bar{\nu}}(\%)$	$N_{exp}^{\nu\bar{\nu}}$	$\epsilon^{\ell^+\ell^-}(\%)$	$N_{exp}^{\ell^+\ell^-}$	N_{exp}^{total}
30	43	75.8	27	16.7	92.6
40	53	35.1	49	11.7	46.8
50	45	10.0	49	3.9	13.9
55	41	4.7	43	1.9	6.5
60	33	1.9	38	0.8	2.6
65	23	0.6	27	0.2	0.8

Table 4: Numbers of events after successive cuts in the muon channel, for the data, for simulated $Z^0 \to q\bar{q}$ events and for a H^0 of mass 60 GeV. The numbers of simulated $Z^0 \to q\bar{q}$ events have been scaled so that the real and simulated data sample sizes are the same. Four-fermion events are not included in this simulation. The numbers between parentheses give efficiencies.

Cuts	Data	$Z^0 \to q\bar{q}$	$\mu^+\mu^- H^0$
Preselection	139481 (7.00%)	149129 (7.49%)	0.82 (81%)
Common	64754 (3.25%)	74523 (3.74%)	0.74 (74%)
μ-pair identification	1658 (0.08%)	2187 (0.11%)	0.65 (65%)
Isolation	15 (0.00%)	0 (0.00%)	0.50 (49%)
Di-lepton Mass	15 (0.00%)	0 (0.00%)	0.41 (41%)
Hadronic Mass	1 (0.00%)	0 (0.00%)	0.41 (41%)

Table 5: Numbers of events after successive cuts in the electron channel, for the data, for simulated $Z^0 \to q\bar{q}$ events and for a H^0 of mass 60 GeV. The numbers of simulated $Z^0 \to q\bar{q}$ events have been scaled so that the real and simulated data sample sizes are the same. Four-fermion events are not included in this simulation. The numbers in parentheses give efficiencies.

Cuts	Data	$Z^0 \to q\bar{q}$	$e^+e^- H^0$
Preselection	139957 (7.03%)	149129 (7.49%)	0.78 (77%)
Common	64978 (3.26%)	74523 (3.74%)	0.68 (68%)
e-pair identification	312 (0.02%)	502 (0.03%)	0.53 (52%)
Isolation	14 (0.00%)	0 (0.00%)	0.41 (41%)
Di-lepton Mass	14 (0.00%)	0 (0.00%)	0.35 (35%)
Hadronic Mass	0 (0.00%)	0 (0.00%)	0.35 (35%)

Table 6: Properties of the event selected in the charged lepton channel. Momenta, masses and energies are expressed in GeV, angles in degrees and distances in millimeters.

Property	Cut Value	Event 15048 Run 4353
p^{μ^-}	5	7.3 $\pm$ 0.2
p^{μ^+}	5	19.3 $\pm$ 0.7
$p^{\mu^+} + p^{\mu^-}$	25	26.6 $\pm$ 0.7
$m_{\mu\mu}$	15	16.6 $\pm$ 0.3
Minimum $\mu^+\mu^-$ opening angle	30	89
Mass of the hadronic system	25	54$\pm$7
Radius of displaced vertex	—	1.6$\pm$0.4
Recoil mass against $\mu\mu$	—	61.2$\pm$1.0
Center-of-mass energy	—	91.17

Figure 1

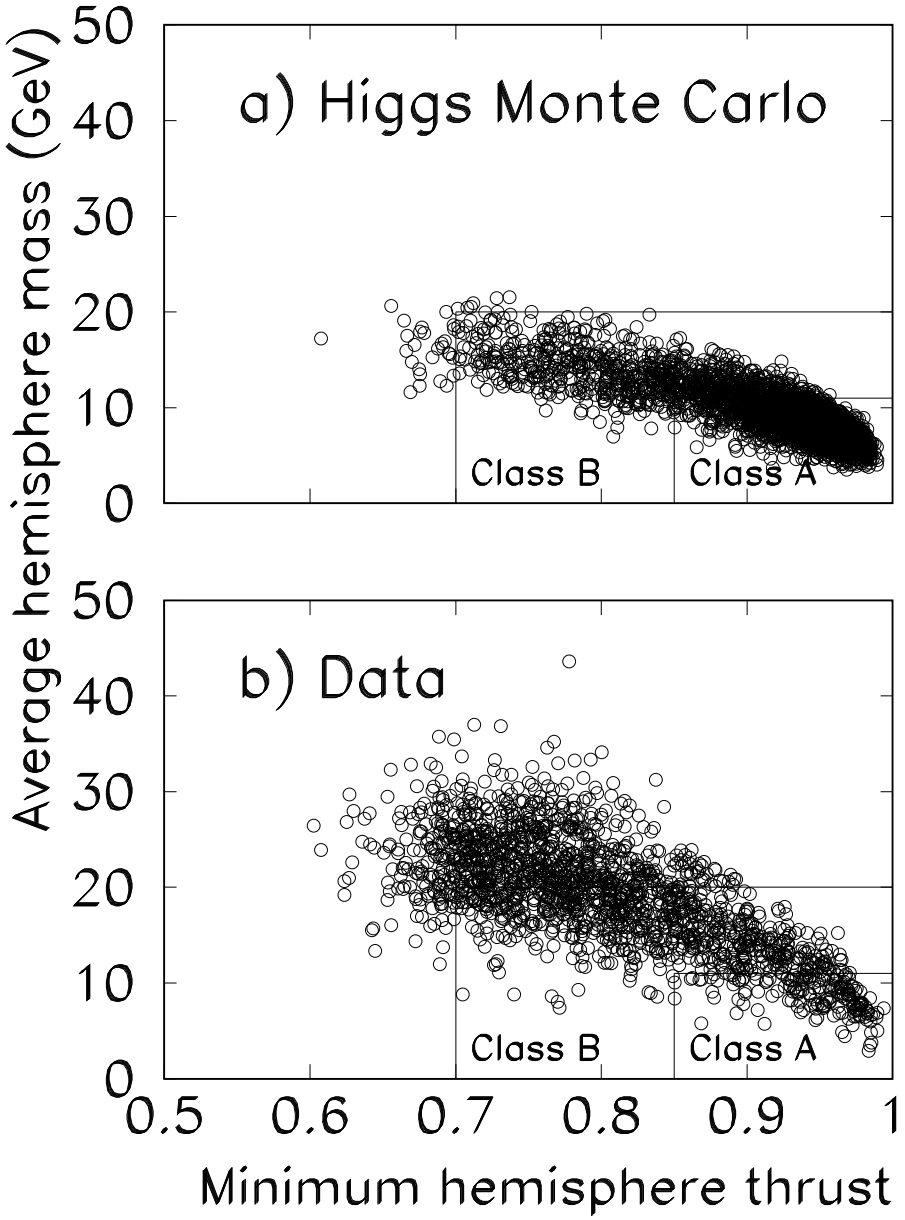

The T_{hemi}^{min} versus m_{hemi}^{avg} distribution for events after all cuts except the final acolinearity and acoplanarity cuts have been applied, for
(a) simulated Higgs boson events with mass 60 GeV,
(b) data.
The boundaries of classes A and B, as described in the text, and table 1, are also shown.

Figure 2

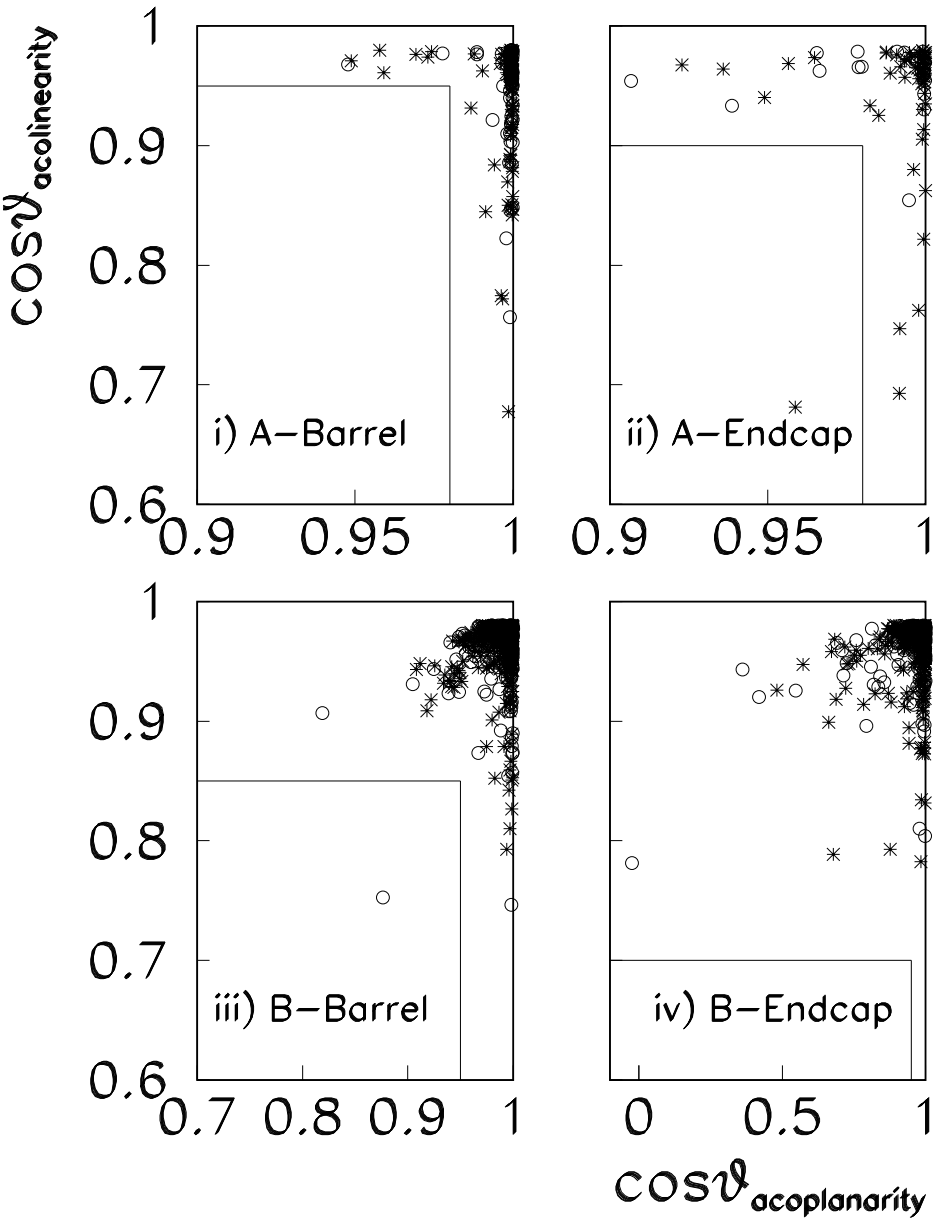

The acolinearity cosine versus acoplanarity cosine for events in classes
(i) A-barrel,
(ii) A-endcap,
(iii) B-barrel,
(iv) B-endcap.
after all other cuts have been applied. The stars represent the data, and the circles represent the simulated hadronic Z^0 decays. The simulated event sample has approximately half the number of events of the data sample. Accepted events lie within the boxes in the lower left of the plots. There are no events (data or simulated data) in the accepted region off the figure scale.

Figure 3

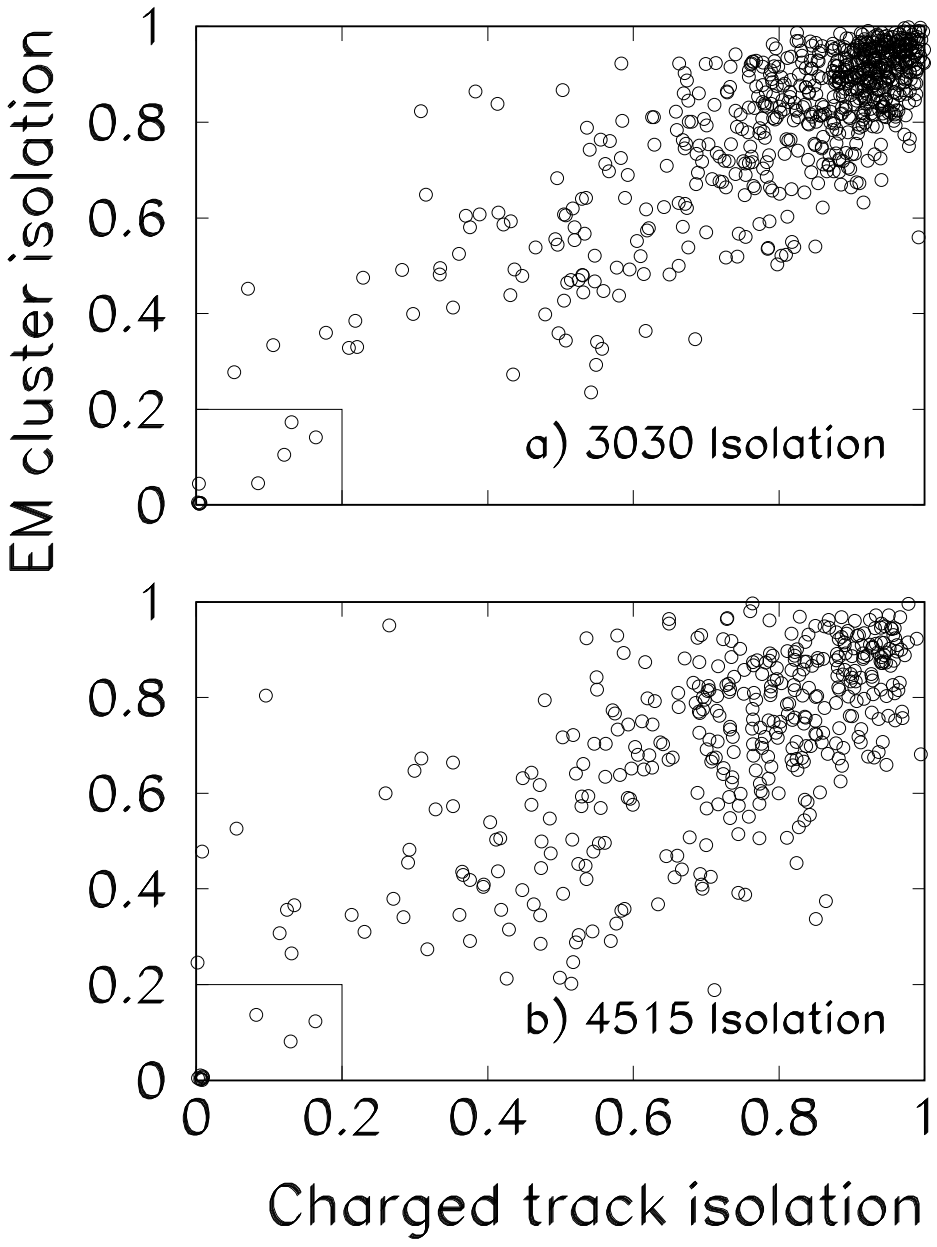

The isolation quality (the fraction of charged track momentum in the isolation cones versus the fraction of electromagnetic calorimeter energy in the isolation cones) for e^+e^- and $\mu^+\mu^-$ pairs found in the data prior to applying the lepton isolation cuts for
(a) 30°–30° cones,
(b) 45°–15° cones.
Events passing these isolation requirements lie within the boxes in the lower left corner of the plots.

Figure 4

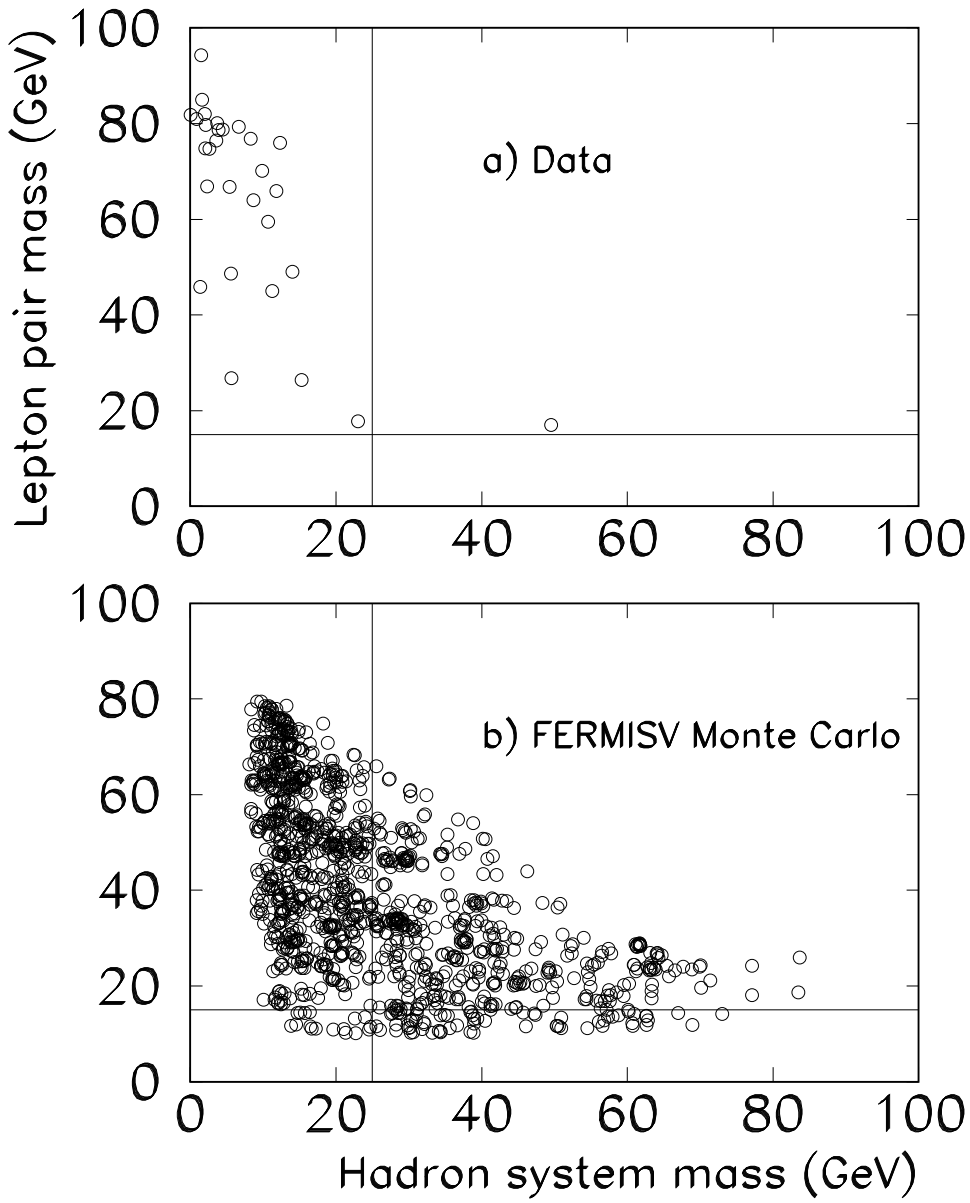

The di-lepton mass versus the mass of the hadronic system after the isolation cuts for
(a) data,
(b) simulated four-fermion events.
The horizontal and vertical lines show the minimum di-lepton and hadronic system masses accepted by the analysis. The number of events in (b) corresponds to 100 times the luminosity of the data sample, and shows the long tail of the hadronic mass distribution. The generator was run with a minimum threshold of 10 GeV on both the di-lepton and hadronic masses. Events with high recoil mass and low di-lepton mass are further suppressed by the requirements on the momentum and opening angle of the pair. The hadronic mass values have been smeared to reproduce the observed recoil mass resolution.

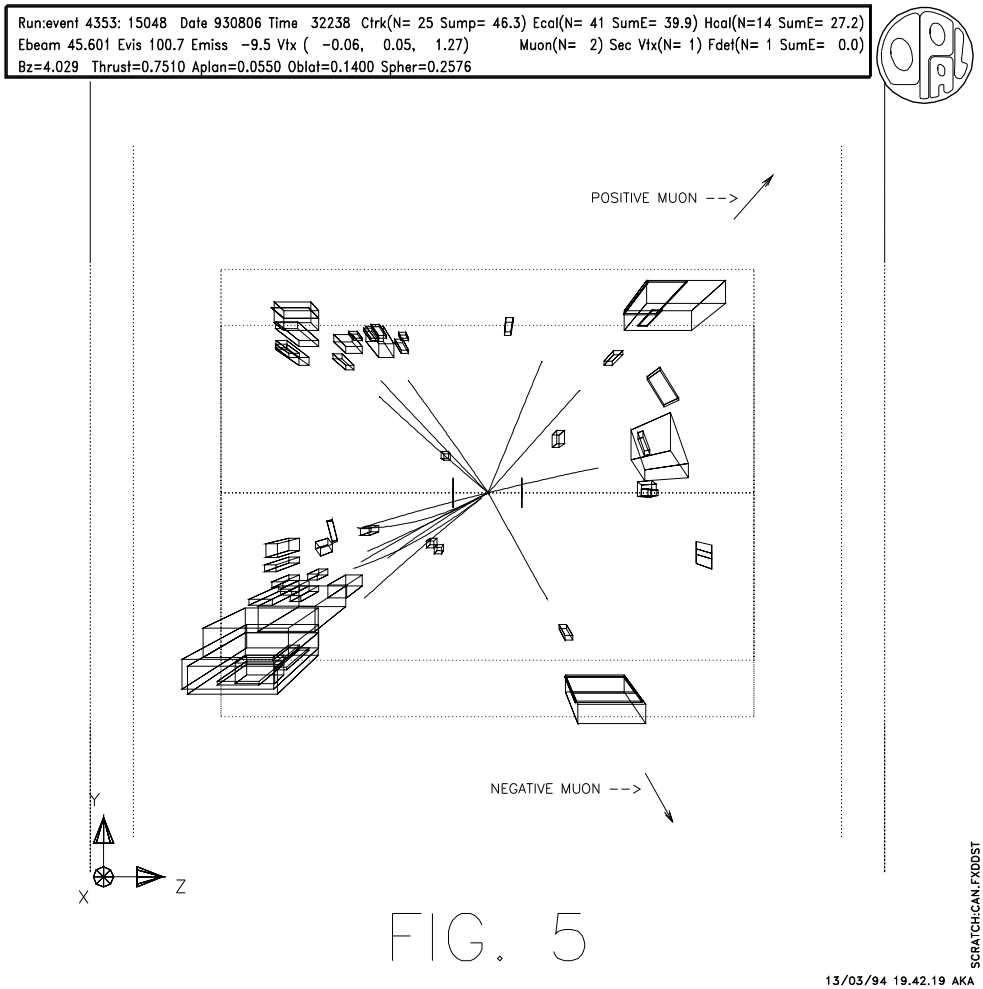

FIG. 5

Display in the y-z plane of the event accepted by the charged lepton channel selection procedure. The tracks and clusters shown pass the data quality cuts. Two jets are seen in the negative z direction. A third jet, consisting of a track and some clusters in the electromagnetic calorimeter, is visible in the positive z direction near the beam pipe. For both muons, the tracks, the associated clusters in the electromagnetic and hadron calorimeters and the track segments in the muon chambers (denoted by arrows) are visible.

Figure 6

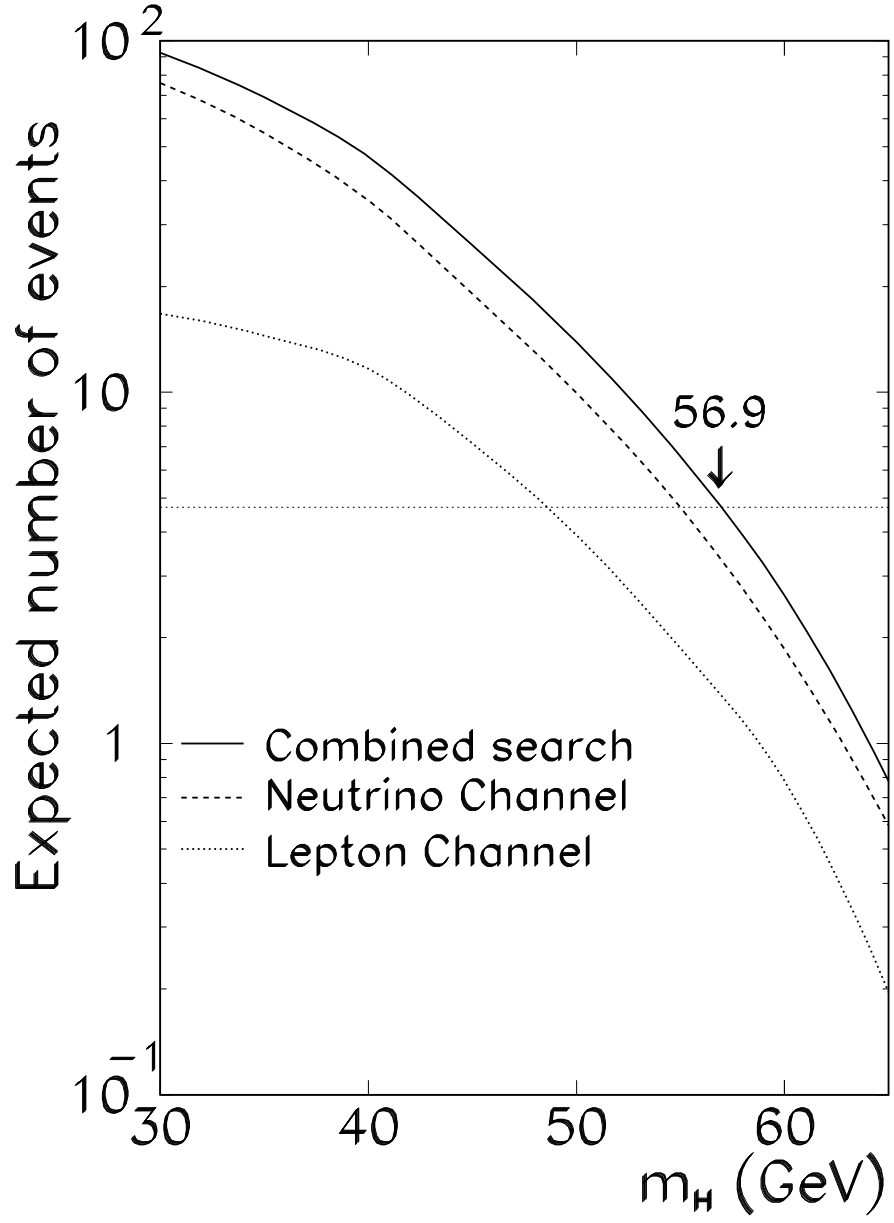

The number of expected Higgs boson events as a function of the Higgs boson mass. The horizontal line shows the number of events required to establish a limit at the 95% confidence level. The dotted line shows the number of expected events in the charged lepton channel, the dashed line shows the number in the neutrino channel, and the solid line shows the sum of expected events in both channels. The arrow shows the new lower limit at 56.9 GeV.